Journal of Molecular Liquids 305 (2020) 112823

Contents lists available at ScienceDirect

Journal of Molecular Liquids

journal homepage: www.elsevier.com/locate/molliq

Dispersion of magnetic susceptibility in a suspension of flexible ferromagnetic rods

M. Molcan [a,*], P. Kopcansky [a], M. Timko [a], M. Rajnak [a], H. Gojzewski [b,c], A. Cēbers [d]

[a] Institute of Experimental Physics, Slovak Academy of Sciences, Watsonova 47, Košice 040 01, Slovakia
[b] University of Twente, Materials Science and Technology of Polymers, Faculty of Science and Technology, Drienerlolaan 5, 7522 NB Enschede, the Netherlands
[c] Poznan University of Technology, Faculty of Materials Engineering and Technical Physics, Piotrowo 3, 60-965 Poznań, Poland
[d] MMML lab, Department of Physics, University of Latvia, Jelgavas 3, Rīga LV-1002, Latvia

ARTICLE INFO

Article history:
Received 16 December 2019
Received in revised form 20 February 2020
Accepted 1 March 2020
Available online 02 March 2020

ABSTRACT

The properties of suspensions of magnetosomes extracted from magnetotactic bacteria are investigated. By using dynamic light scattering and measuring the dispersion of magnetic susceptibility it is shown that sonicated samples with broken magnetosome chains have qualitatively different behavior in comparison with native samples. This is explained by the presence of flexible chains of magnetosomes in non-sonicated samples which have the qualitative features of magnetic susceptibility predicted by the model of flexible magnetic rods.

1. Introduction

Magnetotactic bacteria are an interesting example of an active system in which properties are field dependent [1,2]. The magnetic properties are a product of magnetosome structures, which are defined as intracellular nanocrystals of iron-based magnetic minerals (Fe_3O_4 or Fe_3S_4) enveloped by a phospholipid bilayer membrane [3]. The chain-like arrangement of the magnetosomes allows the individual magnetic moments to add up, which results in magnetic dipolar interactions strong enough to align the cell within the Earth's weak magnetic field [4]. The elasticity of the chain is caused by the phospholipid bilayer which encapsulates and links the magnetic particles. The magneto-elastic properties of magnetosomes have attracted considerable interest, primarily because of applications in magnetic hyperthermia [5–9], drug delivery by magneto-aerotaxis [10,11] and as contrast agents for magnetic resonance imaging [12,13]. For such applications, it is necessary to know how the magnetosomes interact with applied fields. The character of the interaction depends strongly on the bending stiffness of the magnetosome chains [14]. In the case of chains isolated from bacteria the bending stiffness is described by the magnetic interactions between magnetosomes. Such chains often collapse into clusters and closed-ring structures to minimize their magnetic stray field energy [14,15]. The extent to which a chain interacts with the applied field is determined by the number of particles in the chain. In the shorter chains with fewer particles the modified magneto-elastic properties comparing with long chains are expected. Based on these assumptions, we describe the qualitative difference between the response of long and mechanically shortened chains to the applied AC and DC magnetic field using the theoretical model of flexible ferromagnetic rods. We also compare these results with the experimentally measured magnetic properties of the native sample (extracted magnetosome chains) and sample with chains broken by sonication.

2. Material and methods

2.1. Rods material and sample modification method

A suspension of bacteria containing magnetosome particles was used as an experimental material for an AC susceptibility analysis of flexible magnetic rods. Magnetosomes form chain-like magnetic structures in magnetotactic bacteria. In this study magnetite magnetosomes extracted from the magnetotactic bacterium *Magnetospirillum* sp. *strain AMB-1* were used. These bacteria synthesize nano-sized magnetite magnetosomes covered by phospholipid bilayer membranes [9,16,17]. A detailed description of the growth process of the bacteria and the extraction of the magnetosome chain particles is given in Molcan and Dzarova et al. [9,18]. The magnetosome samples were of a distinct length and thus suitable for an investigation into the impact of the rod length and related properties. The sample IM represented the extracted long magnetosome chains dispersed in HEPES buffer. The next sample (SM) was obtained by sonicating the IM magnetosome suspension using a Sonifier Cell Disruptor, Branson Ultrasonics, model 450, USA. Using a micro-tip probe the long chains (magnetic rods) were homogenized and their size distribution shifted to smaller values. The following sonication parameters were applied: a frequency of 20 kHz at 280 W of power for 1 h.

* Corresponding author.
E-mail address: molcan@saske.sk (M. Molcan).

https://doi.org/10.1016/j.molliq.2020.112823
0167-7322/

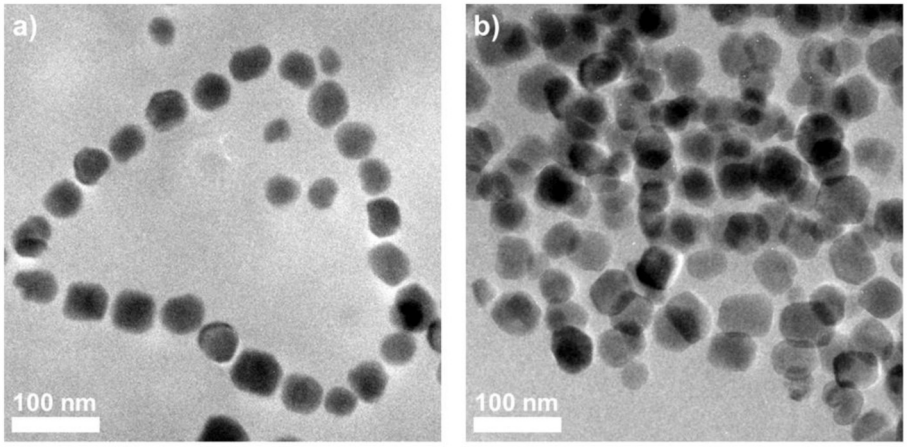

Fig. 1. TEM images of IM and SM magnetosomes.

2.2. Transmission electron microscope (TEM)

The samples were prepared by dropping a micro-droplet of the magnetosome suspension from a syringe with a stainless steel needle on a carbon-coated copper support grid which was then allowed to dry in the air. TEM analysis was performed in a Philips CM300ST FEG Transmission Electron Microscope at an acceleration voltage of 300 kV in a bright field.

2.3. Dynamic light scattering (DLS)

The hydrodynamic size distribution of the magnetosomes was measured by the DLS apparatus Zetasizer Nano ZS (Malvern Instruments, UK) with a 4 mW He—Ne laser, $\lambda = 633$ nm. The scattering angle was 173° and the temperature 25 °C.

2.4. Magnetization measurements

Magnetization measurements of the prepared suspension of magnetosomes were carried out by a Vibrating Sample Magnetometer installed on a cryogen-free superconducting magnet (Cryogenic Ltd., UK). The magnetization curves were measured at room temperature and an applied magnetic field up to 120 kA/m.

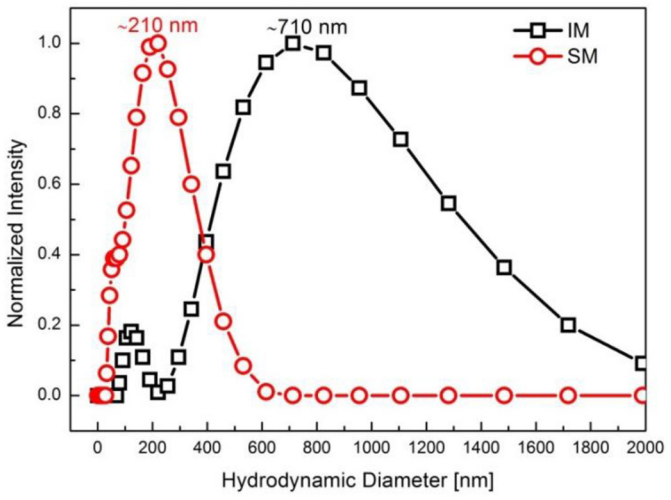

Fig. 2. Normalized distribution of hydrodynamic diameter of IM and SM magnetosomes.

2.5. AC magnetic susceptibility

AC magnetic susceptibility tests were performed on the Imego Dynomag, Acreo Swedish IC, SE susceptometer with the frequency range from 1 Hz up to 250 kHz with a volume susceptibility sensitivity of $4 \cdot 10^{-7}$. The field excitation amplitude was 400 A/m. The magnetosome colloid sample (200 μl) was mounted in a glass vial into the AC susceptometer holder between two sensing coils. The experiment was carried out at room temperature (~22 °C).

3. Experimental results

The effect of the applied sonication on magnetosomes is demonstrated in Fig. 1. Fig. 1a) represents isolated magnetosomes (IM) forming long chains composed of several adjacent particles. A mixture of individual magnetosomes in combination with shortened chains consisting of a few particles per chain is depicted in Fig. 1b) (SM sample).

The noticeable influence of sonication on the chain dimensions was confirmed by DLS measurements as well. The IM sample is characterized by a bimodal size distribution. Except for the dominant peak at 710 nm we can see also a small peak below 200 nm which can be attributed to premature magnetosomes or magnetosomes partially deformed by the extraction. After sonication (SM sample) the character of the size distribution has changed (as shown in Fig. 2), leading to a decrease in the average hydrodynamic diameter to 210 nm which is caused by the rapid increase in the fraction of small particles.

The impact of sonication is also confirmed by magnetization measurements at room temperature (293 K). In the case of the SM sample with a concentration of 1.53 mg/ml of magnetite, we can see well-saturated magnetization already at 10 kA/m. On the other hand, the IM sample with a concentration of 1.03 mg/ml exhibits an increasing magnetization tendency over the range of magnetic field values covered in the experiment (See Fig. 3). This can be associated with the greater magnetic moment of the longer chains. The fast saturation of SM is caused by a lower size distribution and we can also see a diamagnetic contribution originating from the non-magnetic parts of the sample (the HEPES buffer and lipid shells). For both curves zero coercivity is observed as it is typical for nanoparticle colloid systems, for example in ferrofluids [19].

The important difference in the behavior of IM and SM samples is found by measurements of the dispersion of the magnetic AC susceptibility of the samples as shown in Fig. 4. In the case of the IM sample, we can see just a part of the relaxation maximum close to 1 Hz (Fig. 4, upper part). From the shape of the curve it can be deduced that the relaxation peak exists under the frequency range employed in this study. On the

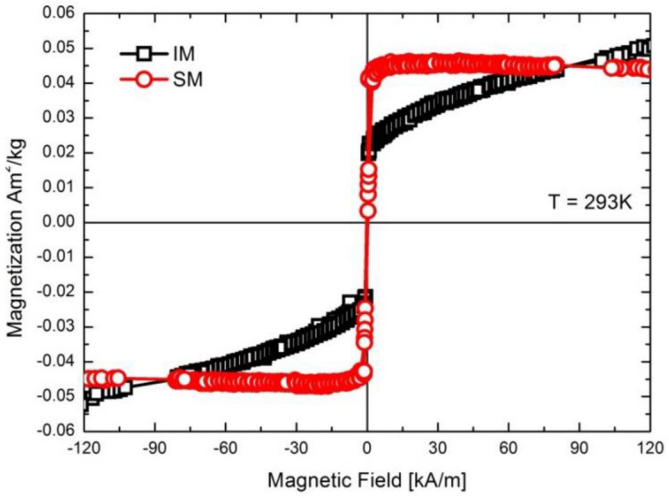

Fig. 3. Magnetization curves of IM and SM magnetosome colloids measured at room temperature (293 K).

other hand, the shortened chains of the SM sample are able to relax even at higher frequencies. The SM sample shows a well-developed relaxation peak, indicating a Brownian relaxation frequency close to 1000 Hz. When the SM sample with broken chains has features similar to Debye dispersion then close values of the real and imaginary parts show monotonous behavior as a function of the frequency.

Using the *DynoMag* software [20] the experimental IM data were fitted according to the "extended multi-core model"

$$\chi(\omega) = \chi_{0_B} \int \frac{1}{(1 + j\omega\tau_B(r_H))} f(r_H) dr_H + \frac{\chi_{0_N}}{1 + (j\omega\tau_N)^{\alpha}} \quad (1)$$

where χ_{0B} is the DC susceptibility for the particles that undergo Brownian relaxation, ω the angular frequency ($2\pi f$), r_H the hydrodynamic radius of the particles, $f(r_H)$ is the hydrodynamic radius distribution function. τ_B is the Brownian relaxation time $\tau_B = (3V_H\eta)/(k_BT)$, where V_H is the hydrodynamic volume, η the viscosity of the liquid the magnetic nanoparticles (magnetosomes) are placed in, k_B the Boltzmann constant ant T is the temperature. The last part in Eq. (1) is the Cole-Cole expression that describes the AC susceptibility contributions from the Néel relaxation. χ_{0N} is the DC susceptibility due to the Néel relaxation, τ_N is the Néel relaxation time and α describes the degree of distribution of the Néel relaxation times (due to the size distribution of the single-domains and/or magnetic interactions between the single-domains) and can have the values $0 \le \alpha \le 1$ [20]. By this fit we finally obtain the hydrodynamic size distribution of the magnetosomes. The IM size distribution is shown in Fig. 5. The obtained value $D_{HYD} = 702$ nm is comparable with the size obtained by DLS = 710 nm. These data are evidence of the presence of large aggregates (possibly chains) in the IM sample. The role of chains in the dispersion of magnetic susceptibility is considered in the next section. Comparable data between DLS (210 nm) and the extended multi-core fit of AC susceptibility (180 nm) were obtained also for the SM sample.

4. Flexible rod model

Experimental data of magnetic susceptibility of samples of magnetosomes may be explained by the model of flexible ferromagnetic rods. In this model the response of a chain of magnetosomes to the polarizing field consists of the deformation of the rod due to the torque from the magnetic field opposed by the elastic torque due to the bending of the rod. Since the magnetosomes are not linked by special linkers we estimate the bending modulus solely from dipolar interactions $K_b = m^2/2d^2$ [21,22], where m is the magnetic moment of the magnetosome and d its diameter.

The model is as follows. The deformation of the rod in the external field $\overrightarrow{H} = (0, H\cos(\omega t), 0)$ making the angle β with the field is described

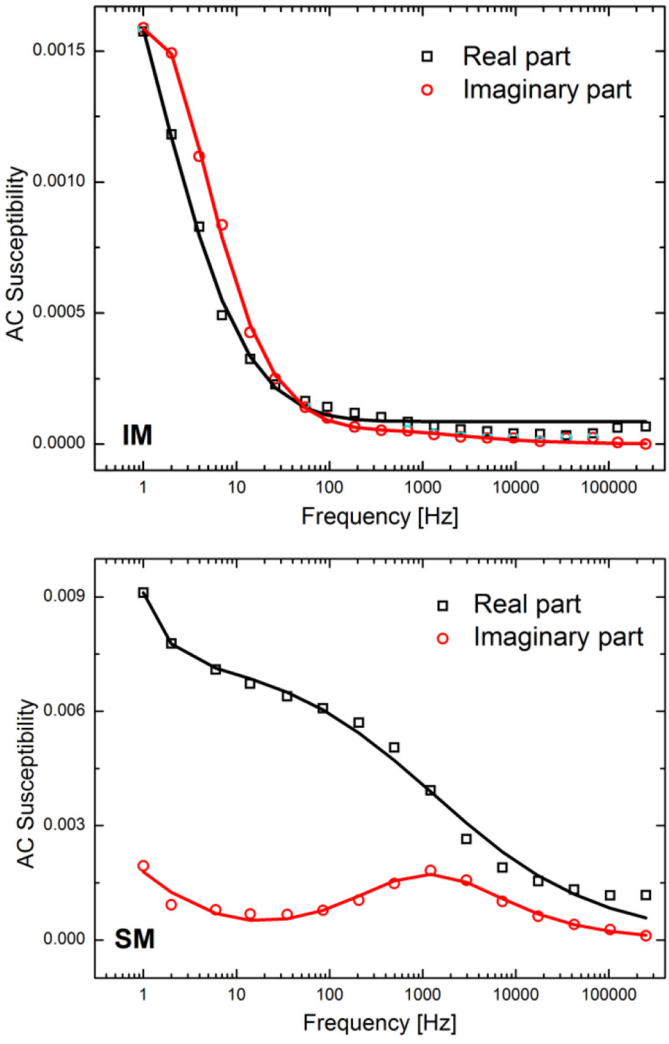

Fig. 4. Real and imaginary part of the AC susceptibility vs frequency of the IM and SM sample. The solid lines are the results of the fitting by the "extended multi-core model".

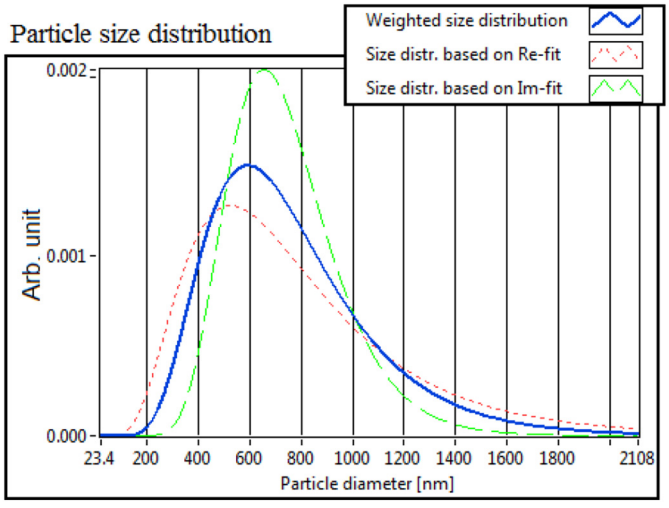

Fig. 5. Hydrodynamic size distribution of isolated sample IM obtained from AC susceptibility data.

by the angle $\vartheta(l)$ (where l is the natural parameter of the centerline) between the tangent vector and the center line of the initial straight configuration (see Fig. 6).

The model of the ferromagnetic rod [23] in the case of small deformation gives (subscript denotes the corresponding partial derivative, $\zeta = 4\pi\eta/(2\ \ln(\frac{2L}{d})-1)$ [24] is the hydrodynamic drag coefficient per unit length of the rod)

$$\zeta\vartheta_{,t} = -K_b\vartheta_{,llll} \tag{2}$$

at boundary conditions corresponding to the free and unclamped ends: absence of the torque $\vartheta_{,l}|_{0,\ L} = 0$ and zero shearing force $-K_b\vartheta_{,ll}|_{0,\ L} - MH\sin(\beta) = 0$, where $M = m/d$ is the magnetization par unit length of the rod and L is its length. The magnetic moment of the rod induced by the polarizing field then reads

$$m_{rod} = M\int_0^L \cos(\beta-\vartheta)dl \cong ML\cos(\beta) + M\sin(\beta)\int_0^L \vartheta(l)dl \tag{3}$$

The first term in Eq. (3) gives the magnetic moment of the straight rod and disappears after taking the average with respect to the isotropic distribution of orientations of the rods.

The following scales are introduced: lengths are scaled with the length L of the rod and time by the characteristic elastic deformation time of the rod in viscous fluid $\tau = \zeta L^4/K_b$. Using relations for ζ, K_b.

and the value given above of the characteristic elastic deformation time at $\eta = 10^{-2}P, m = \frac{\pi}{6}d^3M_s$ (the saturation magnetization of magnetite M_s=500 G) is 7.3 ms. For the characteristic frequency f_* ($2\pi f_*\tau = 1$) we obtain 21.7 Hz. This gives an estimate for the frequency range where the scaling law described below is valid.

The solution of the boundary value problem for Eq. (2) in the steady case when $\vartheta = \tilde{\vartheta}e^{i\omega t}$ in the field $H = H_0e^{i\omega t}$ taking the average with respect to the isotropic distribution of the rods for the magnetic susceptibility reads

$$\chi(\omega) = \chi' - i\chi'' = -\frac{4M^2L^3((1-\cos(p))sh(p) + (ch(p)-1)\sin(p))}{3K_b\ (1-\cos(p)ch(p))p^3} \tag{4}$$

where $p = (\omega\tau)^{1/4}e^{-i\pi/8}$. In the limit $\omega \to 0$ there is a singularity for the imaginary part of the susceptibility $\chi'' = 8M^2L^3/K_b\omega\tau$. It may be regularized by taking into account the Brownian motion when $\chi = \chi_L/(1 + i\omega\tau_B)$, where $\chi_L = (ML)^2/3k_BT$ and the Brownian relaxation time $\tau_B = \zeta L^3/24k_BT$. In the limit $\tau_B \to \infty$ this gives the singular behavior $\chi'' = 8M^2/\omega L\zeta$. We should remark that the bending modulus in this limit cancels out since the rods behave as rigid.

The real and imaginary parts of the magnetic susceptibility normalized by $2M^2L^3/3K_b$ are shown in Fig. 7. It shows that the contribution of the elastic deformations of the rod gives the characteristic Debye type dispersion of magnetic susceptibility. It should be noted that the maximum for the imaginary part appears only when the singular part of it is extracted. If it is taken into account the maximum disappears.

At large $\omega\tau$ relation (4) gives

$$\chi(\omega) = \frac{2^{3/2}M^2L^3}{3K_b}e^{-3i\pi/8}(\omega\tau)^{-3/4} \tag{5}$$

Relation (5) shows that at large $\omega\tau$ the real and imaginary parts of the susceptibility have close values and have the characteristic asymptotics $\chi', \chi'' \sim (\omega\tau)^{-3/4}$. These conclusions may be compared with the experimental data for the IM sample. The experimental data for χ', χ'' in the limited range of the AC field frequencies in the logarithmic coordinates are shown in Fig. 8. The solid line shows the dependence corresponding to $f^{-3/4}$ with a shift for convenience along the y axis . We can remark that the ratio of the imaginary and real parts at least over some frequency range is close to the prediction $\frac{\chi''}{\chi'} = tg(\frac{3\pi}{8})$. This allows us to conclude that the qualitative difference in the behavior of the IM and SM samples is caused by the presence of flexible chainlike aggregates of magnetosomes.

5. Conclusion

Suspensions of native chains of magnetosomes and sonicated samples with broken chains show qualitatively different magnetic dispersion. If sonicated samples show the characteristic Debye like curves of complex susceptibility then a suspension of native samples shows monotonous dependence of the real and imaginary parts on the frequency. This behavior is described by the model of the ferromagnetic rod when the magnetic susceptibility is due to the flexibility of the rod. The

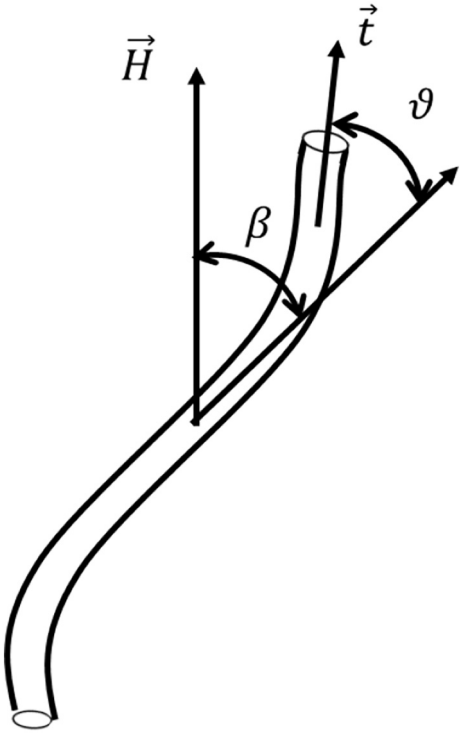

Fig. 6. Sketch of ferromagnetic rod deformation in an applied magnetic field. $\vartheta(l)$ is the angle which the tangent $\vec{t}$ makes with the initial straight configuration characterized by its orientation angle β with the field.

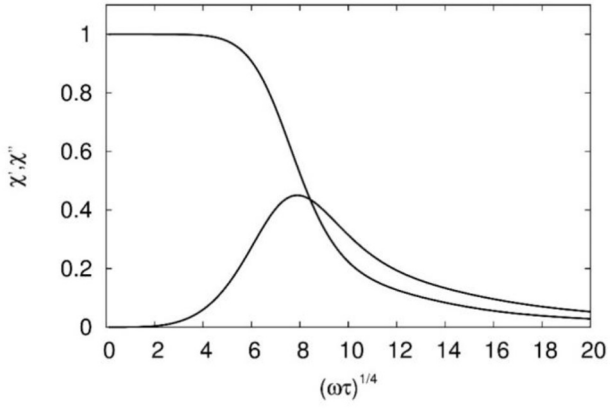

Fig. 7. Real and imaginary parts of the magnetic susceptibility as a function of elastic deformation time of flexible rod model.

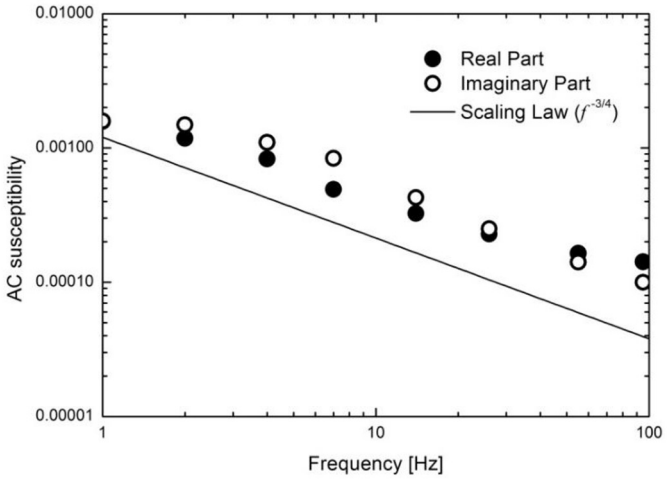

Fig. 8. The real and imaginary parts of the magnetic susceptibility of IM sample as a function of the frequency in logarithmic coordinates. The solid line shows the dependence corresponding to the scaling law $f^{-3/4}$ (with a shift along the *y* axis for convenience).

characteristic scaling law for the complex magnetic susceptibility as a function of the frequency is obtained in the frame of the model and qualitatively corresponds to the experimental data.

CRediT authorship contribution statement

M. Molcan: Resources, Writing - original draft, Writing - review & editing, Investigation. **P. Kopcansky:** Investigation, Writing - review & editing. **M. Timko:** Investigation, Writing - review & editing. **M. Rajnak:** Investigation. **H. Gojzewski:** Investigation. **A. Cēbers:** Writing - original draft, Writing - review & editing, Investigation, Methodology.

Acknowledgments

This work was supported by the project MVTS M-ERA.NET 2 – FMF, MVTS MAGBBRIS, MODEX (ITMS2014+: 313011T548) and by the Slovak Research and Development Agency under the contracts no. APVV-18-0160, APVV-15-0453.. A.C. is supported by M.era-net project FMF No. 1.1.1.5/ERANET/18/04. H.G. acknowledges the Ministry of Science and Higher Education for the project no. 06/62/SBAD/1923 realized at the Faculty of Materials Engineering and Technical Physics, Poznan University of Technology, and the support within the Bekker Programme from the Polish National Agency for Academic Exchange.

References

[1] R. Alonso-Matilla, D. Saintillan, Microfluidic flow actuation using magnetoactive suspensions, EPL (Europhysics Lett) 121 (2018) 24002, https://doi.org/10.1209/0295-5075/121/24002.
[2] B. Vincenti, C. Douarche, E. Clement, Actuated rheology of magnetic microswimmers suspensions: emergence of motor and brake states, Phys. Rev. Fluids. 3 (2018), 033302. https://doi.org/10.1103/PhysRevFluids.3.033302.
[3] G. Vargas, J. Cypriano, T. Correa, P. Leão, D.A. Bazylinski, F. Abreu, Applications of magnetotactic bacteria, magnetosomes and magnetosome crystals in biotechnology and nanotechnology: mini-review, Molecules 23 (2018) https://doi.org/10.3390/molecules23102438.
[4] E. Katzmann, M. Eibauer, W. Lin, Y. Pan, J.M. Plitzko, D. Schüler, Analysis of magnetosome chains in magnetotactic bacteria by magnetic measurements and automated image analysis of electron micrographs, Appl. Environ. Microbiol. 79 (2013) 7755–7762, https://doi.org/10.1128/AEM.02143-13.
[5] E. Alphandéry, S. Faure, L. Raison, E. Duguet, P.A. Howse, D.A. Bazylinski, Heat production by bacterial magnetosomes exposed to an oscillating magnetic field, J. Phys. Chem. C 115 (2011) 18–22, https://doi.org/10.1021/jp104580t.
[6] E. Alphandéry, S. Faure, O. Seksek, F. Guyot, I. Chebbi, Chains of magnetosomes extracted from AMB-1 magnetotactic bacteria for application in alternative magnetic field cancer therapy, ACS Nano 5 (2011) 6279–6296, https://doi.org/10.1021/nn201290k.
[7] M. Timko, M. Molcan, A. Hashim, A. Skumiel, M. Muller, H. Gojzewski, A. Jozefczak, J. Kovac, M. Rajnak, M. Makowski, P. Koƥcanský, Hyperthermic effect in suspension of magnetosomes prepared by various methods, IEEE Trans. Magn. 49 (2013) https://doi.org/10.1109/TMAG.2012.2224098.
[8] M. Molcan, I. Petrenko, M.V. Avdeev, O.I. Ivankov, M. Garamus, A. Skumiel, A. Jozefczak, M. Kubovcikova, P. Kopcansky, M. Timko, Structure characterization of the magnetosome solutions for hyperthermia study, J. Mol. Liq. 235 (2017) https://doi.org/10.1016/j.molliq.2016.12.054.
[9] M. Molcan, H. Gojzewski, A. Skumiel, S. Dutz, J. Kovac, M. Kubovcikova, P. Kopcansky, L. Vekas, M. Timko, Energy losses in mechanically modified bacterial magnetosomes, J. Phys. D. Appl. Phys. 49 (2016) https://doi.org/10.1088/0022-3727/49/36/365002.
[10] O. Felfoul, M. Mohammadi, S. Taherkhani, D. de Lanauze, Y. Zhong Xu, D. Loghin, S. Essa, S. Jancik, D. Houle, M. Lafleur, L. Gaboury, M. Tabrizian, N. Kaou, M. Atkin, T. Vuong, G. Batist, N. Beauchemin, D. Radzioch, S. Martel, Magneto-aerotactic bacteria deliver drug-containing nanoliposomes to tumour hypoxic regions, Nat. Nanotechnol. 11 (2016) 941–947, https://doi.org/10.1038/nnano.2016.137.
[11] J.-B. Sun, J.-H. Duan, S.-L. Dai, J. Ren, L. Guo, W. Jiang, Y. Li, Preparation and antitumor efficiency evaluation of doxorubicin-loaded bacterial magnetosomes: magnetic nanoparticles as drug carriers isolated from *Magnetospirillum gryphiswaldense*, Biotechnol. Bioeng. 101 (2008) 1313–1320, https://doi.org/10.1002/bit.22011.
[12] M. Boucher, F. Geffroy, S. Prévéral, L. Bellanger, E. Selingue, G. Adryanczyk-Perrier, M. Péan, C.T. Lefèvre, D. Pignol, N. Ginet, S. Mériaux, Genetically tailored magnetosomes used as MRI probe for molecular imaging of brain tumor, Biomaterials 121 (2017) 167–178, https://doi.org/10.1016/J.BIOMATERIALS.2016.12.013.
[13] R. Taukulis, M. Widdrat, M. Kumari, D. Heinke, M. Rumpler, É. Tompa, R. Uebe, A. Kraupner, A. Cebers, D. Schueler, M. Pósfai, A.M. Hirt, D. Faivre, Magnetic iron oxide nanoparticles as MRI contrast agents - a comprehensive physical and theoretical study, Magnetohydrodynamics. 51 (2015) 721–748. https://doi.org/10.22364/mhd.51.4.7.
[14] B. Kiani, D. Faivre, S. Klumpp, Elastic properties of magnetosome chains, New J. Phys. 17 (2015), 043007. https://doi.org/10.1088/1367-2630/17/4/043007.
[15] M. Timko, A. Džarová, P. Kopčanský, V. Závišová, M. Koneracká, J. Kováč, A. Šprincová, M. Vaclavíková, L. Ivaničová, I. Vávra, Magnetic properties of magnetite formed by biomineralization and chemical synthesis, Acta Phys. Pol. A 113 (2008) 573–576. https://doi.org/10.12693/APhysPolA.113.573.
[16] T. Matsunaga, Y. Okamura, Y. Fukuda, A.T. Wahyudi, Y. Murase, H. Takeyama, Complete genome sequence of the facultative anaerobic magnetotactic bacterium Magnetospirillum sp. strain AMB-1, DNA Res. 12 (2005) 157–166, https://doi.org/10.1093/dnares/dsi002.
[17] L. Le Nagard, X. Zhu, H. Yuan, K. Benzerara, D.A. Bazylinski, C. Fradin, A. Besson, S. Swaraj, S. Stanescu, R. Belkhou, A.P. Hitchcock, Magnetite magnetosome biomineralization in Magnetospirillum magneticum strain AMB-1: a time course study, Chem. Geol. 530 (2019), 119348. https://doi.org/10.1016/J.CHEMGEO.2019.119348.
[18] A. Dzarova, F. Royer, M. Timko, D. Jamon, P. Kopcansky, J. Kovac, F. Choueikani, H. Gojzewski, J.J. Rousseau, Magneto-optical study of magnetite nanoparticles prepared by chemical and biomineralization process, J. Magn. Magn. Mater. 323 (2011) 1453–1459, https://doi.org/10.1016/J.JMMM.2010.12.041.
[19] Z. Karimi, L. Karimi, H. Shokrollahi, Nano-magnetic particles used in biomedicine: core and coating materials, Mater. Sci. Eng. C. 33 (2013) 2465–2475, https://doi.org/10.1016/J.MSEC.2013.01.045.
[20] DynoMag Instruction Manual, Imego, (n.d.). https://www.acreo.se/our-offer-0/the-dynomag-system-and-the-high-frequency-hf-ac-susceptometer.
[21] A. Cēbers, Flexible magnetic filaments, Curr. Opin. Colloid Interface Sci. 10 (2005) 167–175, https://doi.org/10.1016/J.COCIS.2005.07.002.
[22] D. Vella, E. du Pontavice, C.L. Hall, A. Goriely, The *magneto-elastica*: from self-buckling to self-assembly, Proc. R. Soc. A Math. Phys. Eng. Sci. 470 (2014) 20130609, https://doi.org/10.1098/rspa.2013.0609.
[23] A. Cebers, K. Erglis, Flexible magnetic filaments and their applications, Adv. Funct. Mater. 26 (2016) 3783–3795, https://doi.org/10.1002/adfm.201502696.
[24] D.B. Stein, M.J. Shelley, Coarse graining the dynamics of immersed and driven fiber assemblies, Phys. Rev. Fluids. 4 (2019), 073302. https://doi.org/10.1103/PhysRevFluids.4.073302.